Jpn. J. Appl. Phys. Vol. 42 (2003) pp. L 866–L 868
Part 2, No. 7B, 15 July 2003

Demonstration of X-Ray Talbot Interferometry

Atsushi MOMOSE, Shinya KAWAMOTO[1], Ichiro KOYAMA, Yoshitaka HAMAISHI[1], Kengo TAKAI[2] and Yoshio SUZUKI[2]

Department of Advanced Materials Science, Graduate School of Frontier Sciences, The University of Tokyo, 7-3-1 Hongo, Bunkyo-ku, Tokyo 113-8656, Japan
[1]*Department of Applied Physics, School of Engineering, The University of Tokyo, 7-3-1 Hongo, Bunkyo-ku, Tokyo 113-8656, Japan*
[2]*SPring-8, Mikazuki, Hyogo 679-5198, Japan*

(Received April 18, 2003; accepted for publication May 29, 2003)

First Talbot interferometry in the hard X-ray region was demonstrated using a pair of transmission gratings made by forming gold stripes on glass plates. By aligning the gratings on the optical axis of X-rays with a separation that caused the Talbot effect by the first grating, moiré fringes were produced inclining one grating slightly against the other around the optical axis. A phase object placed in front of the first grating was detected by moiré-fringe bending. Using the technique of phase-shifting interferometry, the differential phase corresponding to the phase object could also be measured. This result suggests that X-ray Talbot interferometry is a novel and simple method for phase-sensitive X-ray radiography. [DOI: 10.1143/JJAP.42.L866]

KEYWORDS: Talbot effect, hard X-rays, radiography, interferometry, differential phase

The potential of phase-sensitive X-ray radiography has been widely noted particularly for observations of structures with small variation of X-ray absorption coefficient which are hard to be imaged by conventional X-ray radiography. Several methods for phase-sensitive X-ray radiography have been studied mainly using synchrotron radiation, the development of which enabled us to use a brilliant X-ray beam with sufficient spatial coherency.

Phase-sensitive X-ray radiography would be classified into three types that generate contrast approximately corresponding to (1) $\cos\Phi$,[1–3] where Φ is the X-ray phase shift, using a crystal X-ray interferometer,[4] (2) differential phase $\partial\Phi/\partial x$,[5–9] where x denotes a direction perpendicular to the optical axis, and (3) $\nabla^2\Phi$.[10,11]

The generated contrast is normally recorded as it is for instance on an X-ray film. In observing complex objects, however, it is occasionally difficult to understand structures simply from the generated contrast. The determination of the spatial distribution of the X-ray phase shift $\Phi(x, y)$ caused by a sample from the generated contrast is therefore a meaningful next step for quantitative understanding. A successful determination of $\Phi(x, y)$ was first reported[12] using the crystal X-ray interferometer, which was soon combined with X-ray computed tomography, enabling three-dimensional observation of biological soft tissues without using contrast media.[12–15] Later using the method of the type (3), phase-contrast tomography was also achieved[16] in the same manner. These developments are broadening the possible applications of phase-sensitive X-ray radiography.

In this paper, we propose and demonstrate X-ray Talbot interferometry as a novel and simple method for phase-sensitive X-ray radiography that has a potential for medical applications. As described below, this method is classified in the type (2), and the measurement of the differential phase is also demonstrated.

The principle of Talbot interferometry[17–19] is based on the Talbot effect,[20] or a self-imaging phenomenon by a periodic object, for instance a transmission grating, under spatially coherent illumination. It is characteristic of the Talbot effect that one can observe the appearance and disappearance of the grating's self-image along the optical axis. This phenomenon is understood as Fresnel diffraction by the grating.

Expressing complex transmission function $T(x)$ of a grating with a Fourier series as

$$T(x) = \sum_n a_n \exp\left(i2\pi \frac{nx}{d}\right), \tag{1}$$

where a_n is the amplitude of the nth harmonic and d is the period of the grating, the wave field $E(x, z)$ generated behind the grating under unit-amplitude plane wave illumination is given by

$$\begin{aligned} E(x,z) &= \frac{1}{\sqrt{i\lambda z}} \int T(x') \exp\left[\frac{i\pi}{\lambda z}(x-x')^2\right] dx' \\ &= \sum_n a_n \exp\left(-i\pi \frac{n^2 z\lambda}{d^2}\right) \exp\left(i2\pi \frac{nx}{d}\right) \end{aligned} \tag{2}$$

with paraxial approximation, where λ is the wavelength. Here, the optical axis is parallel to the z axis, and the grating is on the (x, y) plane ($z = 0$). The grooves of the gratings are assumed to be parallel to the y axis.

It should be noted that $E(x, z)$ equals $T(x)$ when $z = md^2/\lambda$ (m: even integer). This implies that self-images are generated at the distances (Talbot distances). When m is odd, $E(x, z) = T(x + d/2)$, and similar self-images are also observed. When a phase grating is used ($T(x) = \exp[i\phi(x)]$), one cannot see a contrast at the distances. However, the phase modulation is converted to the modulation of intensity at $z = (m + 1/2)d^2/\lambda$ given[21] by

$$|E(x, z)|^2 = 1 + \sin[\phi(x) - \phi(x + d/2)], \tag{3}$$

which is a case of the so-called fractional Talbot effect.

Next, assuming the illumination with a unit-amplitude nonplane wave expressed with $\exp[i\Phi(x, y)]$, eq. (2) is rewritten as

$$\begin{aligned} E(x,y,z) = \sum_n a_n &\exp\left(-i\pi \frac{n^2 z\lambda}{d^2}\right) \\ &\times \exp\left[i2\pi \frac{n}{d}\left(x - z\varphi(x,y)\right)\right], \end{aligned} \tag{4}$$

where

$$\varphi(x,y) = \frac{\lambda}{2\pi} \frac{\partial\Phi(x,y)}{\partial x}. \tag{5}$$

Equation (4) implies that the self-images are deformed

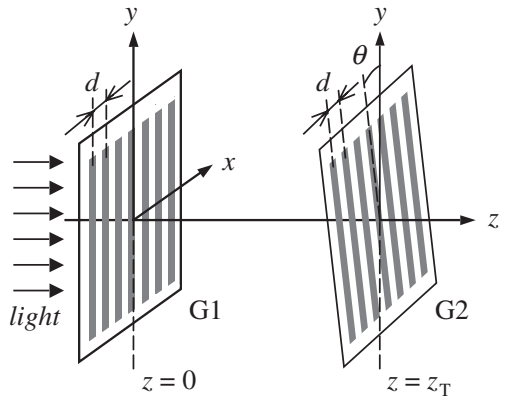

Fig. 1. Schematic of a Talbot interferometer using two transmission gratings.

depending on $\varphi(x, y)$ in proportion to z.

As shown in Fig. 1, Talbot interferometry employs a second grating (G2), whose period is normally the same as that of the first grating (G1), at the (fractional) Talbot distance z_T from G1. When G2 is slightly inclined by θ ($\ll 1$) about the optical axis against G1, one can observe moiré fringes as a superposition of the self-image of G1 and the pattern of G2. The spacing of the moiré fringes is $\sim d/\theta$ under plane-wave illumination. When the incident wavefront is curving because of $\varphi(x, y)$, bent moiré fringes are generated. The $\varphi(x, y)$ is evaluated from the fringes with $\varphi(x, y) \simeq \xi(x, y)\theta/z_T$, where $\xi(x, y)$ is the fringe displacement in the y direction.

In general when the gratings have symmetric structures, the moiré fringes are given by

$$I(x, y, z_T) = b_o c_o + 2 \sum_{n>0} b_n c_n \cos A(x, y, z_T), \tag{6}$$

$$A(x, y, z_T) = 2\pi \frac{n}{d} \{y\theta + z_T \varphi(x, y) + \chi\}, \tag{7}$$

where b_n and c_n are the nth Fourier coefficients of the self-image of G1 and the intensity transmission function of G2, respectively. χ is the displacement of one grating against the other in the x direction.

The Talbot effect and Talbot interferometry were studied extensively in the visible light region and used for wavefront sensing.[22] Several years ago, the fractional Talbot effect in the hard X-ray energy region was demonstrated using third-generation synchrotron radiation with a phase grating.[23]

Aiming at the first demonstration of X-ray Talbot interferometry, we prepared gold gratings of 2 mm × 2 mm area with a pitch of 4 microns (Howa Sangyo Co., Ltd). Stripes were made on 150-μm glass plates by forming grooves 1.25 μm in depth and 1.55 μm in width. It is found from eq. (3) that the contrast of the self-image produced by a phase grating is maximum when the amplitude of spatial phase modulation is $\pi/2$. The depth mentioned above was selected in line with this fact.

First, we checked the self-imaging phenomenon with the grating at the medium-length beamline BL20XU of the third-generation synchrotron radiation facility SPring-8, Japan, where undulator X-rays were available 245 m downstream from the source point through a Si 111 double-crystal monochromator. The X-ray beam size (FWHM) was 4.0 mm (horizontal) × 2.2 mm (vertical). Images were recorded behind the grating using 0.1-nm X-rays with a CCD detector (Hamamatsu Photonics K.K., C4880-50) coupled with optical lens and a phosphor screen, whose effective pixel size was 0.54 μm, varying the axial distance between the grating and the detector. Figures 2(a), 2(c) and 2(e) are images under the self-imaging condition for the phase grating; that is, $z = 8$ cm, 24 cm, and 40 cm, respectively, while for $z = 16$ cm and 32 cm, the contrast of stripes is disappearing as shown in Figs. 2(b) and 2(d), respectively. Because the grating modulated not only the phase but also the amplitude to some extent, the position of full-disappearance was found 1 cm upstream from Fig. 2(b) as shown in Fig. 2(f). Each image was recorded with a 1.2 s exposure.

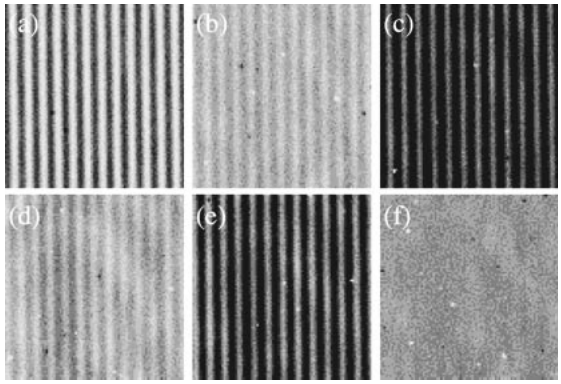

Fig. 2. Images recorded behind the grating. The distances from the grating were 8 cm (a), 16 cm (b), 24 cm (c), 32 cm (d), and 40 cm (e). In addition, a full-disappearance image recorded 15 cm (f) behind the grating is presented. Exactly the same position of the grating could not be monitored in these images owing to the parallelism error of the linear mechanism for changing the grating-detector distance against the optical axis. Therefore, the transition of the self-image between $T(x)$ and $T(x + d/2)$ (see text) is not seen in this result.

Next, we placed another grating at $z = 40$ cm where the self-imaging was observed. According to the principle of Talbot interferometry, it is better to employ an amplitude grating for the second grating. In principle, 100% fringe visibility can be achieved. However, it is not easy to fabricate an amplitude grating in the hard X-ray region. The same grating as the first was therefore used in this experiment relying on the amplitude modulation by the grating, which was calculated to be 19%.

Experiments were performed placing a plastic sphere 1.2 mm in diameter in front of G1 as a phase object generating the phase shift $\Phi(x, y)$. In this experiment, we do not need to resolve individual stripes of the self-image as in Fig. 2. Therefore, the effective pixel size of the X-ray image detector was changed to 6.33 μm by replacing the coupling lens. The detector was located 12 cm behind G2 and moiré fringes were recorded with a 0.4 s exposure. The G2-detector distance was negligible because it was much smaller than the z_T calculated from the moiré fringe spacing, and the generated moiré pattern was unaltered in the propagation at that distance.

As shown in Fig. 3(a), because G2 was inclined against G1 about the optical axis by one degree, moiré fringes were generated and the phase gradient introduced by the phase object was detected as the displacement of the moiré fringes. This result coincides with a simulated image shown in Fig.

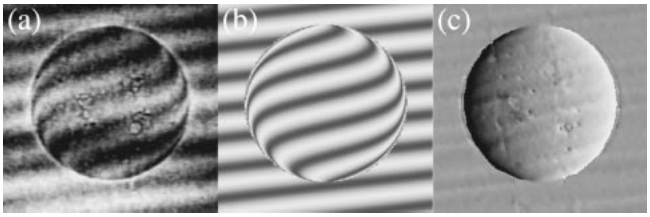

Fig. 3. Images describing the result of the X-ray Talbot interferometry. A moiré image (a) was obtained by placing a plastic sphere (1.2 mm in diameter) as a phase object in front of the first grating. The observed image is consistent with a simulated image (b). An image (c) mapping $\varphi(x, y)$ was measured with the phase-shifting technique. The structures inside the sphere correspond to bubbles.

3(b), where the refractive index of the sphere was assumed to be $1 - 1.61 \times 10^{-6}$, except that the observed fringe visibility was about 30% worse than expected, which might be due to the figure error of the gratings.

Because the X-ray beam was not strictly a plane wave, the moiré fringes in Fig. 3(a) out of the sphere region were not horizontal. The image in Fig. 3(b) was simulated taking account of this fact by adding a term xz_T/R in the braces of eq. (7), where R is the radius of curvature of the X-ray wavefront.

If gratings with a sinusoidal profile are used, the moiré fringes are approximately sinusoidal. Then, $\varphi(x, y)$ can be measured more systematically than $\xi(x, y)\theta/z_T$ by combining the Talbot interferometry with a phase-shifting technique. For instance, by changing the displacement χ in eq. (7) by a step of d/M (M is an integer over 2), one can obtain moiré patterns:

$$I_k(x, y, z_T) \simeq b_o c_o + 2b_1 c_1 \cos\left[\frac{2\pi}{d}\left(y\theta + z_T\varphi(x, y) + \frac{k}{M}d\right)\right]. \quad (k = 1, 2, \cdots, M) \tag{8}$$

Then, $\varphi(x, y)$ is determined with

$$y\theta + z_T\varphi(x, y) \simeq \arg\left[\sum_{k=1}^{M} I_k(x, y, z_T) \exp\left(-i2\pi\frac{k}{M}\right)\right]. \tag{9}$$

Using square-profile gratings, moiré fringes with a triangular profile are generated. Then, the procedure described above cannot be adopted. Although the gratings used in this experiment were fabricated intending to make rectangular grooves for convenience, the generated moiré fringes shown in Fig. 3(a) were approximately sinusoidal as a result. This was consistent with the observation with optical laser microscopy showing that the grating profile was dull. Therefore, we tested the determination of $\varphi(x, y)$ by the phase-shifting technique with the procedure described above. As shown in Fig. 3(c), a resultant image mapping $\varphi(x, y)$ is reasonable.

It is worthwhile from a practical point of view to point out that the use of partial coherent X-rays would also be effective for applying eq. (9). The nth harmonic diffracted by G1 is deflected by $n\lambda z_T/d$ at G2. If the deflection exceeds the spatial coherence length, higher harmonics do not contribute to the Talbot effect and moiré fringe formation. Therefore, under illumination of partially coherent X-rays particularly when z_T is large, approximately sinusoidal moiré fringes are generated and eq. (9) is applicable. The spatial coherence length of the X-rays used in the experiment was estimated to be about 11 μm, which was calculated with $\lambda R'/2\pi w$, where w (= 0.3 mm) was the frond-end slit size in the x (horizontal) direction and R' (= 214 m) corresponded to the distance between G1 and the front-end slit. (The horizontal source size was larger than w.) It is therefore speculated that this mechanism also favored the measurement of Fig. 3(c).

Other methods[5–8] that generate a contrast related to $\varphi(x, y)$ (type (2)) use Bragg diffraction with crystals. Therefore, an X-ray plane wave with a monochromaticity of about 10^{-4} is used as a matter of fact at synchrotron radiation facilities. It should be noted that X-ray Talbot interferometry would be practical with spherical X-rays in virtue of its crystal-free optics. Furthermore, X-rays of a wide band width from a laboratory source are available if partial spatial coherency is assured to some extent. As mentioned above, complete spatial coherency is not always required, and partially coherent X-rays are rather desirable for quantitative measurement with the phase-shifting technique. Provided that a large amplitude grating is developed for G2, these features of X-ray Talbot interferometry would promise feasible applications particularly in the field of medicine.

The experiments reported in this paper were carried out under the approvals of the SPring-8 committee, 2002B0233-NM-np and 2003A0458-NML2-np. This study was partially supported by a grant from the award of Konica Imaging Science Foundation.

1) U. Bonse and M. Hart: Appl. Phys. Lett. **7** (1965) 99.
2) M. Ando and S. Hosoya: *Proc. 6th Int. Conf. X-ray Optics & Microanalysis* (Univ. Tokyo Press, Tokyo, 1972) pp. 63–68.
3) A. Momose and J. Fukuda: Med. Phys. **22** (1995) 375.
4) U. Bonse and M. Hart: Appl. Phys. Lett. **6** (1965) 105.
5) J. Davis, D. Gao, T. E. Gureyev, A. W. Stevenson and S. W. Wilkins: Nature **373** (1995) 595.
6) D. Chapman, W. Thomlinson, R. E. Johnston, D. Washburn, E. Pisano, N. Gmür, Z. Zhong, R. Menk, F. Arfelli and D. Sayers: Phys. Med. Biol. **42** (1997) 2015.
7) M. Ando, H. Sugiyama, A. Maksimenko, W. Pattanasiriwisawa, K. Hyodo and Z. Xiaowei: Jpn. J. Appl. Phys. **40** (2001) L844.
8) C. David, B. Nöhammer and H. H. Solak: Appl. Phys. Lett. **81** (2002) 3287.
9) Y. Kohmura, T. Ishikawa, H. Takano and Y. Suzuki: J. Appl. Phys. **93** (2003) 2283.
10) A. Snigirev, I. Snigireva, V. Kohn, S. Kuznetsov and I. Schelokov: Rev. Sci. Instrum. **66** (1995) 5486.
11) S. W. Wilkins, T. E. Gureyev, D. Gao, A. Pogany and A. W. Stevenson: Nature **384** (1996) 335.
12) A. Momose: Nucl. Instrum. & Methods A **352** (1995) 622.
13) A. Momose, T. Takeda and Y. Itai: Nat. Med. **2** (1996) 473.
14) F. Beckmann, U. Bonse, F. Busch and O. Günnewig: J. Comput. Assist. Tomogr. **21** (1997) 539.
15) A. Yoneyama, A. Momose, I. Koyama, E. Seya, T. Takeda, Y. Itai, K. Hirano and K. Hyodo: J. Synchrotron Rad. **9** (2002) 277.
16) P. Cloetens, W. Luding, J. Baruchel, D. Van Dyck, J. Van Landuyt, J. P. Guigay and M. Schlenker: Appl. Phys. Lett. **75** (1999) 2912.
17) S. Yokozeki and T. Suzuki: Appl. Opt. **10** (1971) 1575.
18) A. W. Lohmann and D. E. Silva: Opt. Commun. **2** (1971) 413.
19) E. Keren and O. Kafri: J. Opt. Soc. Am. A **2** (1985) 111.
20) H. Talbot: Philos. Mag. **9** (1836) 401.
21) J. P. Guigay: Opt. Acta **18** (1971) 677.
22) K. Patorski: *Progress in Optics XXVII* (Elsevier, Amsterdam, 1989).
23) P. Cloetens, J. P. Guigay, C. De Martino and J. Baruchel: Opt. Lett. **22** (1997) 1059.